Letter

Mean-field theory of chaotic insect swarms

R. González-Albaladejo

Departamento de Matemática Aplicada, Universidad Complutense de Madrid, 28040 Madrid, Spain
and Gregorio Millán Institute for Fluid Dynamics, Nanoscience and Industrial Mathematics,
Universidad Carlos III de Madrid, 28911 Leganés, Spain

L. L. Bonilla[*]

Gregorio Millán Institute for Fluid Dynamics, Nanoscience and Industrial Mathematics,
Universidad Carlos III de Madrid, 28911 Leganés, Spain
and Department of Mathematics, Universidad Carlos III de Madrid, 28911 Leganés, Spain

The harmonically confined Vicsek model displays qualitative and quantitative features observed in natural insect swarms. It exhibits a scale-free transition between single and multicluster chaotic phases. Finite-size scaling indicates that this unusual phase transition occurs at zero confinement [Phys. Rev. E **107**, 014209 (2023)]. While the evidence of the scale-free-chaos phase transition comes from numerical simulations, here we present its mean-field theory. Analytically determined critical exponents are those of the Landau theory of equilibrium phase transitions plus dynamical critical exponent $z = 1$ and a new critical exponent $\varphi = 0.5$ for the largest Lyapunov exponent. The phase transition occurs at zero confinement and noise in the mean-field theory. The noise line of zero largest Lyapunov exponents informs observed behavior: (i) the qualitative shape of the swarm (on average, the center of mass rotates slowly at the rate marked by the winding number and its trajectory fills compactly the space, similarly to the observed condensed nucleus surrounded by vapor) and (ii) the critical exponents resemble those observed in natural swarms. Our predictions include power laws for the frequency of the maximal spectral amplitude and the winding number.

Collective animal motion has common features that suggest underlying principles beyond biological details [1–5]. Indeed, insect swarms, fish schools, bird and sheep flocks, or crowds of people exhibit collective properties distinct from those of their component individuals. In the past, these properties have been characterized as of hypnotic [6] or telepathic [7] nature, although other authors in those years argued that the spread of impulse in well-organized groups was adequate to explain the existence of a collective mind of the flock [8]. More recently, advances in stereo videography and calibration [9] have generated enormous amounts of quantitative data for collective animal motion [5]. In particular, the observation of power laws and critical exponents in biological systems [3,10–14] has generated much theoretical investigation into the unusual phase transitions which may be responsible for them. Power laws for natural insect swarms are deduced from correlation functions [14–17]. Their relation to possible renormalization group theories of phase transitions [18] have led to efforts to identify their postulated universality class [17,19–22].

Besides observations in natural settings, mating swarms of male midges have been much studied in laboratory conditions [5,23–28]. Midges perceive acoustic signals and move with low-frequency maneuvers but react with synchronized high-frequency oscillatory motion to the presence of nearby insects [24]. When undriven, the swarm center of mass moves *almost randomly* on a plane (with larger fluctuations in the vertical direction of gravity) but it follows an elliptic trajectory when driven at 1 Hz frequency superimposed to the sound of a male midge [25]. Motions of single midges in swarms follow Lévy walks [29], which might indicate chaotic motion in related animal patterns [30]. Acoustic interaction of midges has been modeled by adaptive gravity, which produces an effective harmonic potential near the swarm center [26]. Swarms comprise a core condensed phase surrounded by a dilute vapor phase with midges entering and leaving the core [27], while individual midges do not sample the swarm uniformly [28]. The long-range correlations between midges in the wild [14–17] are not observed in laboratory conditions where background noise and atmospheric conditions are absent [31].

Finding models accounting for all the different swarm features is challenging. Recently, we have discovered a phase transition in the harmonically confined Vicsek model (HCVM), characterized by scale-free chaos, which exhibits several observed traits of the swarm (condensed nucleus and vapor phases, flatness at the origin and, on a bounded interval, collapse of dynamic correlation function in terms of time divided by correlation length) and is compatible with observed critical exponents [32]. For finitely many insects, the scale-free-chaos phase transition is a critical line separating single from multicluster chaotic swarms, and having correlation length proportional to swarm size. This line converges to zero confinement as insect number goes to infinity and chaos disappears [32]. Since our findings are based on numerical simulations, it is important to have a theory to
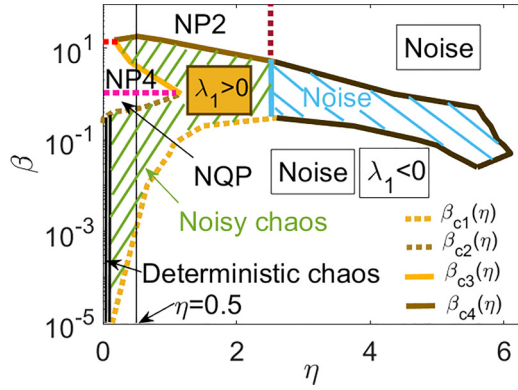
---
[*]Corresponding author: bonilla@ing.uc3m.es

FIG. 1. Phase diagram on confinement vs noise plane indicating regions of deterministic and noisy chaos, noisy period-σ (NPσ) and noisy quasiperiodic (NPQ) attractors, and mostly noise. $M = v_0 = 1$.

interpret them. Not having a renormalization group theory of the HCVM scale-free-chaos phase transition, we develop here a mean-field theory of the HCVM as a first step. Note that the standard Vicsek model with periodic boundary conditions [4,33] displays an ordering transition [34] that is very different from the HCVM scale-free-chaos transition [32].

The three dimensional (3D) HCVM satisfies

$$\mathbf{x}_i(t+1) = \mathbf{x}_i(t) + \mathbf{v}_i(t+1), \quad i = 1, \ldots, N,$$

$$\mathbf{v}_i(t+1) = v_0 \mathcal{R}_\eta \left\{ \Theta \left[\sum_{|\mathbf{x}_j - \mathbf{x}_i| < R_0} \mathbf{v}_j(t) - \beta \mathbf{x}_i(t) \right] \right\}, \quad (1)$$

where $\Theta(\mathbf{x}) = \mathbf{x}/|\mathbf{x}|$, R_0 is the radius of the sphere of influence about particles, β is the confining spring constant, and $\mathcal{R}_\eta(\mathbf{w})$ performs a random rotation uniformly distributed around $\mathbf{w}$ with maximum amplitude of η [32]. First, we set $\eta = 0$, average these equations using the definition

$$\langle f(\mathbf{x}_i) \rangle = \frac{1}{N} \sum_{i=1}^{N} f(\mathbf{x}_i), \quad \mathbf{X}(t) = \langle \mathbf{x}_i \rangle, \quad (2)$$

in the limit as $N \to \infty$, and assume the mean-field (tree [35]) approximation $\langle f(\mathbf{x}_i) \rangle \approx f(\langle \mathbf{x}_i \rangle)$. The result is

$$\mathbf{X}(t+1) - \mathbf{X}(t) = v_0 \Theta[\mathbf{X}(t) - \mathbf{X}(t-1) - \tilde{\beta}\mathbf{X}(t)], \quad (3)$$

where $\tilde{\beta} = \beta/M$ and M is the average number of particles within the sphere of influence about i, all of which remain inside the sphere. We have used that, for a compact swarm, $\langle \sum_{|\mathbf{x}_j - \mathbf{x}_i| < R_0} \mathbf{v}_j(t) \rangle = \langle \sum_{|\mathbf{x}_j - \mathbf{x}_i| < R_0} [\mathbf{x}_j(t) - \mathbf{x}_j(t-1)] \rangle \approx M[\langle \mathbf{x}_i(t) \rangle - \langle \mathbf{x}_i(t-1) \rangle] = M[\mathbf{X}(t) - \mathbf{X}(t-1)]$. Moreover, the initial positions $\mathbf{X}(0)$ and $\mathbf{X}(1)$ characterize a plane to which all successive positions given by (3) belong. This is similar to observed swarm motion [25]. Restoring the alignment noise in (3), we obtain the *stochastic mean-field HCVM* (MFHCVM):

$$\mathbf{X}(t+1) = \mathbf{X}(t) + \mathbf{V}(t+1), \quad (4a)$$

$$\mathbf{V}(t+1) = v_0 \mathcal{R}_\eta \{ \Theta[\mathbf{V}(t) - \tilde{\beta}\mathbf{X}(t)] \}. \quad (4b)$$

Numerical simulations of the MFHCVM produce the phase diagram in Fig. 1. For $\eta = 0$, deterministic chaos with positive largest Lyapunov exponent (LLE) λ_1 occurs on the interval
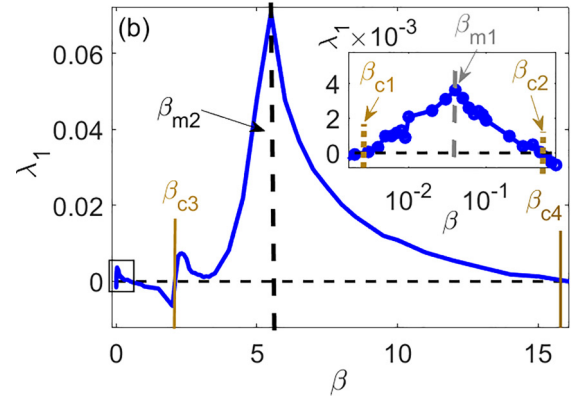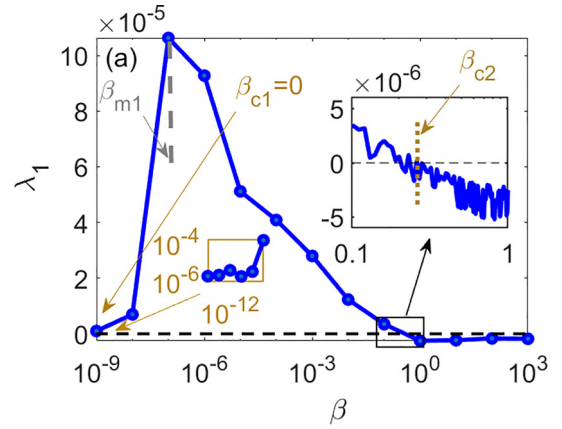

FIG. 2. Largest Lyapunov exponent versus confinement for (a) $\eta = 0$ and (b) $\eta = 0.5$ showing the windows of deterministic and noisy chaos, respectively. The insets show zooms of the rectangular regions in the main figures of each panel.

$(0, \beta_{c2})$. For nonzero noise, noisy chaos (as defined from scale-dependent Lyapunov exponents [32,36]) appears on the intervals $(\beta_{c1}(\eta), \beta_{c2}(\eta))$ and $(\beta_{c3}(\eta), \beta_{c4}(\eta))$, whereas noisy quasiperiodic and periodic attractors exist elsewhere [37]. At $\beta = \eta = 0$, $\lambda_1 = 0$. For $2 < \eta < 2\pi$, noise dominates even though there is a region of chaos swamped by noise for intermediate values of β. For the MFHCVM, the scale-free-chaos phase transition of the 3D HCVM [32] corresponds to the origin in Fig. 1.

Figure 2 shows the windows of positive LLE for vertical lines in Fig. 1 at noises $\eta = 0$ and $\eta = 0.5$, corresponding to deterministic and noisy chaos, respectively. For zero noise, the chaotic window ends at $\beta_{c2} = 0.2$ and begins at $\beta_{c1} = 0$ (in our simulations, we still get a clearly positive LLE at $\beta = 10^{-9}$). There are two chaotic windows (β_{c1}, β_{c2}) and (β_{c3}, β_{c4}) for $\eta = 0.5$ in Fig. 2(b). Inside these windows, the LLE has peaks at β_{m1} and β_{m2}, respectively. Figure 1 shows that the scale-free-chaos phase transition is located at the origin of the phase diagram (β, η). While we can reach this transition by lowering β at $\eta = 0$, we can also move on the critical line $\beta_{c1}(\eta)$ in Fig. 1 and let $\eta \to 0$ until we reach the origin. This latter route to the scale-free-chaos phase transition is reminiscent of finite-size scaling for the HCVM, which produces critical exponents by letting $N \to \infty$ on the critical lines $\beta_c(N; \eta)$ as $\beta_c \to 0+$ having fixed η on the region of noisy chaos [32]. The critical exponents obtained by
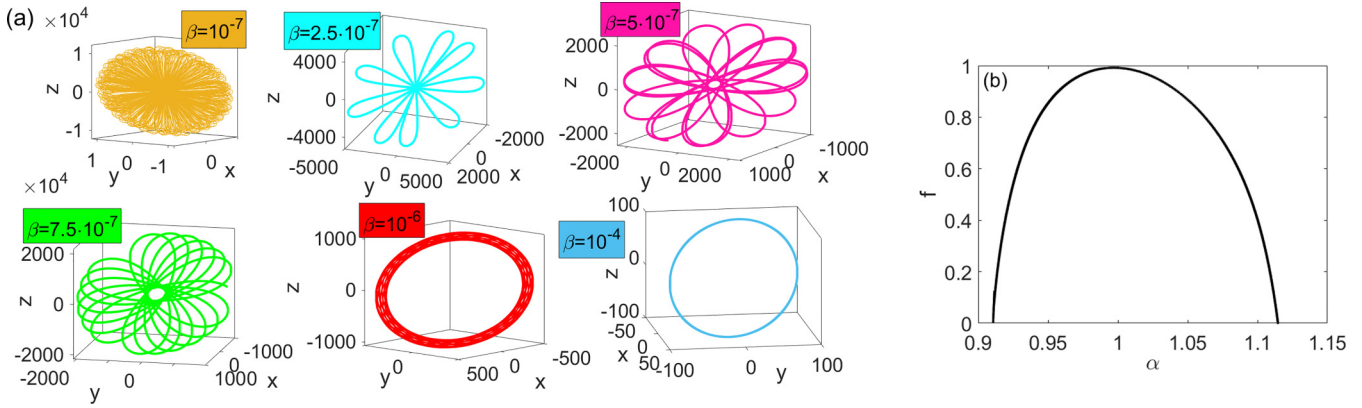
FIG. 3. Deterministic dynamics. (a) Chaotic attractors (depicted on a short time interval) for different values of β. (b) Multifractal singularity spectrum for the transition between quasiperiodicity and chaos.

either route are the same but the deterministic route is more amenable to theory, whereas the critical exponents obtained by descending through the noise line $\beta_{c1}(\eta)$ in Fig. 1 follow from numerical simulations. The maximum at $\beta_{m1} \approx 10^{-7}$ in Fig. 2(a) is in a region of chaotic attractors filling a large portion of space (for $\beta < 10^{-6}$). The chaotic attractors fill a smaller annular region for $\beta > 10^{-6}$; see Fig. 3(a). Attractors filling large regions of space have zero average position and velocity but nonzero time-averaged amplitudes $\langle |\mathbf{X}(t)|^2 \rangle_t$, $\langle |\mathbf{V}(t)|^2 \rangle_t = v_0^2$.

Figure 3(b) shows the singularity spectrum $f(\alpha)$ [38–40] of the transition from quasiperiodicity to chaos at $\beta_{c2}(0)$ of Fig. 2(a). Its shape is that of the circle map, with a maximum $D_0 = \max_\alpha f(\alpha) = 1$ equating the Haussdorff fractal dimension at the transition. The zeros $D_\infty < D_{-\infty}$ of $f(\alpha)$ do not take on the same values as those for the golden-mean winding number of the critical circle map, $D_\infty \approx 0.6326$ and $D_{-\infty} \approx 1.8980$ [38]: $(D_\infty, D_{-\infty})$ is narrower for the undriven transition between quasiperiodicity and chaos at $\beta_{c2}(0)$.

We now find the critical exponents at $\beta = 0$, which correspond to the scale-free-chaos phase transition of the HCVM [32]. In the latter, the correlation length ξ is proportional to swarm size, which can be defined as the time average of

$R(t) = |\mathbf{X}(t)|$ [37]. From (4a), we obtain

$$v_0^2 = |\mathbf{X}(t)|^2 + |\mathbf{X}(t+1)|^2 - 2|\mathbf{X}(t)| \, |\mathbf{X}(t+1)| \cos\theta(t+1)$$
$$= R(t)^2 + R(t+1)^2 - 2R(t)R(t+1)\cos\theta(t+1),$$

where $\theta(t+1)$ is the angle between $\mathbf{X}(t)$ and $\mathbf{X}(t+1)$. Averaging over time and ignoring fluctuations,

$$\langle R(t)^2 \rangle_t \approx \langle R(t) \rangle_t^2, \; \langle R(t)R(t+1)\cos\theta(t+1) \rangle_t$$
$$\approx \langle R(t) \rangle_t^2 \cos\langle \theta(t) \rangle_t = \langle R(t) \rangle_t^2 \cos(2\pi w),$$

where w is the winding number [37]. Thus, we get $v_0^2 \approx 2\langle R \rangle_t^2 [1 - \cos(2\pi w)]$. As $\beta \to 0+$, $w \to 0$ (see Fig. 4), and therefore $\langle R(t) \rangle_t \to \infty$ with

$$w \sim \frac{v_0}{2\pi \langle R \rangle_t}. \tag{5}$$

For zero noise, winding number and the frequency of the highest peak of the power spectrum, $\Omega = w$, for a signal $s(t) = X(t) + Y(t) + Z(t)$ coincide; see Fig. 4(a). Ω is the reciprocal correlation time, therefore (5) implies $\tau \sim \xi$ (relating correlation time and length), and the dynamical critical exponent is $z = 1$. For nonzero noise, the relation between winding number and peak frequency Ω is more complex; see
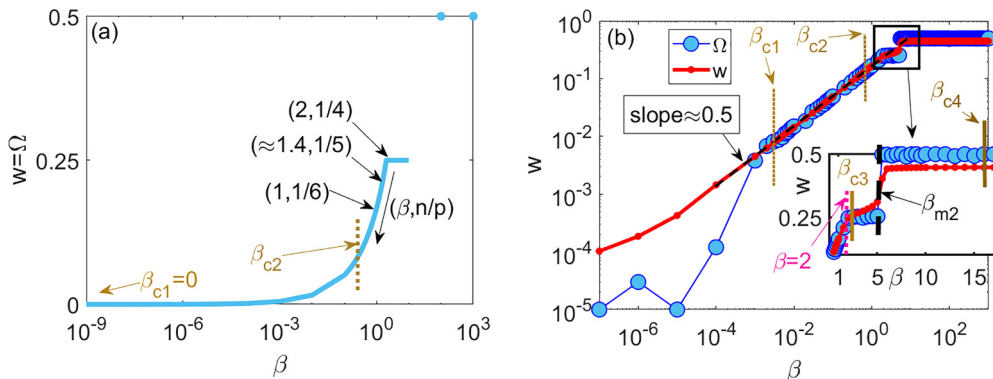

FIG. 4. Winding number versus confinement for (a) $\eta = 0$, (b) $\eta = 0.5$ indicating periodic, quasiperiodic attractors and ends of the chaotic windows as β decreases.
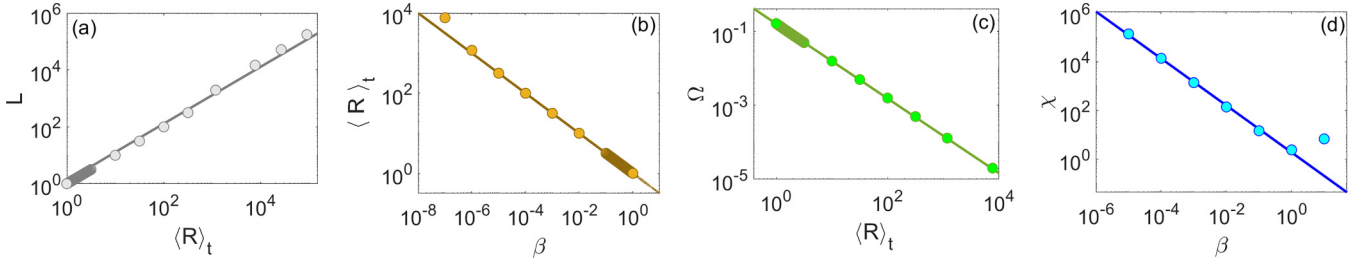
FIG. 5. Power laws for the deterministic case $\eta = 0$ as we approach zero confinement, which corresponds to the scale-free-chaos transition of the harmonically confined Vicsek model. (a) The maximum swarm size, $L = \max(R)$, and the correlation length, $\xi = \langle R \rangle_t$, are proportional. (b) The correlation length scales as $\xi \sim \beta^{-\nu}$ with $\nu = 0.5$. (c) The relation between the frequency for the maximum of the power spectrum scales as $\Omega \sim L^{-z}$ with the dynamic critical exponent $z = 1.01 \pm 0.01$, and (d) the susceptibility scales as $\chi \sim \beta^{-\gamma}$ with $\gamma = 1.000 \pm 0.002$.

Fig. 4(b). Within the first chaotic window, (β_{c1}, β_{c2}), $\Omega = w$, whereas $\Omega < w$ for $\beta < \beta_{c1}$. Within the second chaotic window, (β_{c3}, β_{c4}), Ω is piecewise constant, with a finite jump at β_{m2}, corresponding to the maximum of the LLE. The winding number is smooth: It is slightly larger than Ω for $\beta_{c3} < \eta <$

β_{m2}), and it is slightly smaller than Ω for $\beta_{m2} < \beta < \beta_{c4}$); see the inset of Fig. 4(b).

To obtain the other critical exponents, we note that the order parameter of the MFHCVM cannot be the polarization because $|\mathbf{V}(t)|/v_0 = 1$. For $\eta = 0$, (4b) yields

$$R(t+1)^2 = R(t)^2 + v_0^2 + 2v_0 \frac{(1-\tilde{\beta})R(t)^2 - R(t)R(t-1)\cos\theta(t)}{\sqrt{(1-\tilde{\beta})^2 R(t)^2 + R(t-1)^2 - 2R(t)R(t-1)(1-\tilde{\beta})\cos\theta(t)}}.$$

Time averaging this expression and ignoring fluctuations,

$$0 = v_0^2 + 2v_0 \langle R \rangle_t \frac{1 - \tilde{\beta} - \cos(2\pi w)}{\sqrt{2(1-\tilde{\beta})[1 - \cos(2\pi w)] + \tilde{\beta}^2}}.$$

In the limit as $\beta \to 0+$, $\langle R \rangle_t \to \infty$, $w \to 0$, and this equation yields $1 - \cos(2\pi w) \sim \tilde{\beta} - v_0 \sqrt{2[1 - \cos(2\pi w)]}/(2\langle R \rangle_t)$, from which

$$w \sim \sqrt{\frac{\tilde{\beta}}{4\pi^2}}. \tag{6}$$

Thus, we have found the relation $w \sim \beta^b$, with $b = 1/2$, for the winding number, which plays the role of order parameter in the Landau theory. From (5) and (6), we find the critical exponent $\nu = 1/2$ in the relation $\xi \sim \beta^{-\nu}$. We define the susceptibility χ as the time-averaged norm of the linear response matrix $\mathcal{H}_t = \nabla_{\mathbf{H}} \chi_t = \partial \chi_t^i / \partial H_j$ (at zero field) to an external force resulting from replacing $\mathbf{V}(t) + \mathbf{H}$ instead of the alignment force $\mathbf{V}(t)$ in (4b) [37]:

$$\chi = \langle \|\mathcal{H}_t\| \rangle_t, \quad \|\mathcal{H}_t\| = \sqrt{\lambda_M(\mathcal{H}_t \mathcal{H}_t^T)}. \tag{7}$$

Here $\lambda_M(\mathcal{H}_t \mathcal{H}_t^T)$ is the maximum eigenvalue of the symmetric positive matrix $\mathcal{H}_t \mathcal{H}_t^T$. Equation (4a) produces $\mathbb{Y}_{t+1} = \mathbb{Y}_t + \mathbb{W}_{t+1}$, where $\mathbb{Y}^{ij} = (\mathbf{Y}^j)_i = \partial \mathbf{X}_i / \partial H_j$, and $\mathbb{W}^{ij} = (\mathbf{W}^j)_i = \partial \mathbf{V}_i / \partial H_j$, at $\mathbf{H} = \mathbf{0}$. Equation (4b) yields [37]

$$\left(\mathbf{W}_{t+1}^j\right)_i = \mathcal{R}_\eta \left\{ \mathbb{A}_t^{ik} \left[\left(\mathbf{W}_t^j\right)_k - \frac{\beta}{M}\left(\mathbf{Y}_t^j\right)_k \right] + \mathbb{A}_t^{ik}(\delta^j)_k \right\},$$

$$(\delta^j)_i = \delta_{ij}, \tag{8a}$$

$$\mathbb{A}_t = \frac{v_0}{\left|\mathbf{V}(t) - \frac{\beta}{M}\mathbf{X}(t)\right|}$$

$$\times \left\{ \mathbb{I} - \frac{\left[\mathbf{V}(t) - \frac{\beta}{M}\mathbf{X}(t)\right]\left[\mathbf{V}(t) - \frac{\beta}{M}\mathbf{X}(t)\right]^T}{\left|\mathbf{V}(t) - \frac{\beta}{M}\mathbf{X}(t)\right|^2} \right\}. \tag{8b}$$

Here sum over repeated indices is understood. A modification of the argument leading to (6) produces $\chi \sim \frac{\partial \langle R \rangle_t}{\partial H}|_{H=0} \sim \beta^{-\gamma}$ with critical exponent $\gamma = 1$ [37]. Hence, the critical exponents of the MFHCVM are the same as those in the Landau
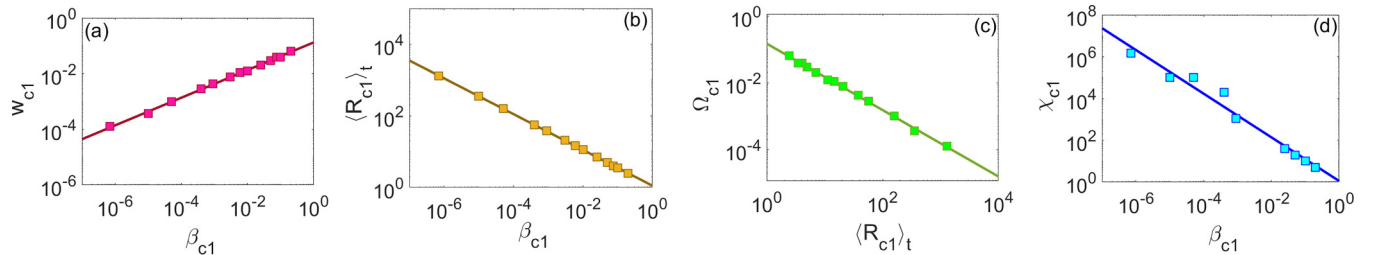

FIG. 6. Same as Fig. 5 for the stochastic case with $\beta = \beta_{c1}(\eta)$ and $\eta \to 0$. (a) Power law for the order parameter, which is the winding number, versus β, $w \sim \beta^b$, with $b = 0.497 \pm 0.006$; (b) Correlation length $\xi \sim \beta^{-\nu}$ with $\nu = 0.500 \pm 0.001$; (c) dynamic critical exponent $z = 0.99 \pm 0.01$ for the law $\Omega \sim \xi^{-z}$; (d) susceptibility vs confinement $\chi \sim \beta^{-\gamma}$ with $\gamma = 1.04 \pm 0.06$.
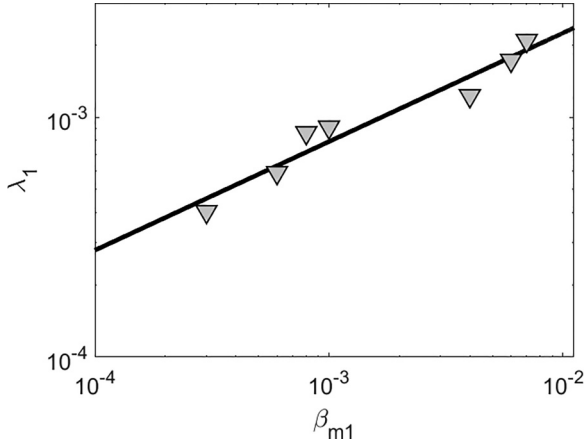
FIG. 7. LLE vs $\beta_{m1}(\eta)$, the location of the local maximum of the LLE at each value of the noise (stochastic MFHCVM) as $\eta \to 0$. The power law is $\lambda_1 \sim \beta^\varphi$ with critical exponent $\varphi = 0.45 \pm 0.05$, which is compatible with the predicted value 0.5.

theory of phase transitions [41]:

$$\nu = b = 0.5, \quad \gamma = 1, \qquad (9)$$

with dynamical critical exponent $z = 1$. Figure 5 exhibits power laws with critical exponents (9) and $z = 1$ as obtained from numerical simulations. As we approach the origin in Fig. 1 through the line $\beta_{c1}(\eta)$ ($\eta \to 0$), we obtain the same critical exponents from numerical simulations, as shown in Fig. 6.

For the deterministic and stochastic cases, the swarm size $L = \max_t R(t)$ is proportional to the time-averaged length of the center-of-mass position as the confinement decreases; see Fig. 5(a). Thus, swarm size and correlation length are proportional. Figures 6(a) shows the power law of the winding number, $w_{c1} \sim \beta_{c1}^b$, $b \approx 0.5$. Figures 5(b) and 6(b) plot the correlation length power law with critical exponent $\nu = 0.5$. The dynamical critical exponent z is found from the relation $\Omega \sim \xi^{-z}$, $z = 1.01 \pm 0.01$, between the frequency corresponding to the maximum of the power spectrum and the correlation length; see Figs. 5(c) and 6(c). Last, the power laws for the susceptibility are shown in Figs. 5(d) and 6(d).

In Ref. [37], we find the bound $\lambda_1 \geqslant \sqrt{\beta}$ for the LLE. Assuming LLE satisfies a power law $\lambda_1 \sim \beta^\varphi$, we obtain $\varphi \leqslant 0.5$. Finite velocity propagation implies $\varphi \geqslant \nu$ [32], and therefore $\varphi = \nu = 0.5$. This value agrees with numerical simulations yielding $\lambda_1(\beta_{m1})$ as $\beta_{c1}(\eta) \to 0$; see Fig. 7. The mean-field critical exponents are different from those of the HCVM, but they are close to them: $z = 1$ is the same and the relation $\varphi = z\nu$ holds for both models [32].

In conclusion, we have proposed a mean-field theory of the harmonically confined Vicsek model. It consists of a map for the 3D position and velocity of the swarm center of mass. The map displays transitions from quasiperiodicity to chaos and a confinement-noise phase diagram that is comparable to that of the HCVM [32]. The phase diagram exhibits a scale-free-chaos phase transition at vanishing noise that is similar to that of the HCVM (winding number replaces polarization as order parameter). Its critical exponents are those of the Landau theory of equilibrium phase transitions [41] plus $z = 1$ and $\varphi = z\nu$ for the LLE power law. The noise shifts the chaotic interval to $(\beta_{c1}(\eta), \beta_{c2}(\eta))$ with $\lim_{\eta \to 0} \beta_{c1}(\eta) = 0$ but numerical simulations show that the critical exponents are the same as in the deterministic case [37]. The deduced critical exponents of the mean-field theory are the same for any space dimension $d > 1$. We shall show elsewhere that the scale-free-chaos phase transition exists for $d = 2$ but not for $d = 1$. What are the consequences of the scale-free phase transition for real insect swarms? This transition occurs at zero confinement and noise in the mean-field theory. Its unfolding on the zero LLE noise line of Fig. 1(a) informs observed behavior: qualitative shape of the swarm (on average, the center of mass rotates slowly at the rate marked by the winding number and its trajectory fills compactly a space region, akin to a condensed nucleus surrounded by vapor [27]; see Figs. 19(b) of Ref. [32] and S3 of Ref. [37]), and critical exponents similar to those observed in natural swarms. The frequency of the maximal spectral amplitude and the winding number could be extracted from experimental data. As the line of zero LLE in Fig. 1 merges with that of the scale-free-chaos transition for infinitely many particles [32], it also corresponds to the same phase transition. The study of this transition at the verge of chaos for finitely many particles will be tackled in the future. A worthwhile endeavor would be reconstructing a noisy chaotic attractor from the swarm center of mass data (both in the wild or in the laboratory) by using the same techniques as in the numerical simulations in Ref. [32].

[1] A. Okubo, Dynamical aspects of animal grouping: Swarms, schools, flocks, and herds, Adv. Biophys. **22**, 1 (1986).

[2] J. K. Parrish and L. Edelstein-Keshet, Complexity, pattern, and evolutionary trade-offs in animal aggregation, Science **284**, 99 (1999).

[3] D. J. T. Sumpter, *Collective Animal Behavior* (Princeton University Press, Princeton, NJ, 2010).

[4] T. Vicsek, A. Zafeiris, Collective motion, Phys. Rep. **517**, 71 (2012).

[5] N. T. Ouellette, A physics perspective on collective animal behavior, Phys. Biol. **19**, 021004 (2022).

[6] G. Le Bon, *Psychologie des foules* (Germer Baillière, Paris, 1895).

[7] W. J. Long, *How Animals Talk: And Other Pleasant Studies of Birds and Beasts* (Bear & Co., Rochester, Vermont, 1919).

[8] R. C. Miller, The mind of the flock, Condor **23**, 183 (1921).

[9] D. H. Theriault, N. W. Fuller, B. E. Jackson, E. Bluhm, D. Evangelista, Z. Wu, M. Betke, and T. L. Hedrick, A protocol and calibration method for accurate multi-camera field videography, J. Exp. Biol. **217**, 1843 (2014).

[10] T. Mora, W. Bialek, Are biological systems poised at criticality? J. Stat. Phys. **144**, 268 (2011).

[11] W. S. Bialek, *Biophysics: Searching for Principles* (Princeton University Press, Princeton, NJ, 2012).

[12] Q.-Y. Tang, Y. Y. Zhang, Y. Wang, W. Wang, D. R. Chialvo, Critical Fluctuations in the Native State of Proteins, Phys. Rev. Lett. **118**, 088102 (2017).

[13] M. Azaïs, S. Blanco, R. Bon, R. Fournier, M.-H. Pillot, and J. Gautrais, Traveling pulse emerges from coupled intermittent walks: A case study in sheep, PLoS One **13**, e0206817 (2018).

[14] A. Cavagna, I. Giardina, T. S. Grigera, The physics of flocking: Correlation as a compass from experiments to theory, Phys. Rep. **728**, 1 (2018).

[15] A. Attanasi, A. Cavagna, L. Del Castello, I. Giardina, S. Melillo, L. Parisi, O. Pohl, B. Rossaro, E. Shen, E. Silvestri, and M. Viale, Collective behaviour without collective order in wild swarms of midges, PLoS Comput. Biol. **10**, e1003697 (2014).

[16] A. Attanasi, A. Cavagna, L. Del Castello, I. Giardina, S. Melillo, L. Parisi, O. Pohl, B. Rossaro, E. Shen, E. Silvestri, and M. Viale, Finite-Size Scaling as a Way to Probe Near-Criticality in Natural Swarms, Phys. Rev. Lett. **113**, 238102 (2014).

[17] A. Cavagna, D. Conti, C. Creato, L. Del Castello, I. Giardina, T. S. Grigera, S. Melillo, L. Parisi, and M. Viale, Dynamic scaling in natural swarms, Nat. Phys. **13**, 914 (2017).

[18] K. G. Wilson, The renormalization group and critical phenomena, Rev. Mod. Phys. **55**, 583 (1983).

[19] L. Chen, J. Toner, C. F. Lee, Critical phenomenon of the order-disorder transition in incompressible active fluids, New J. Phys. **17**, 042002 (2015).

[20] L. Chen, C. F. Lee, J. Toner, Incompressible polar active fluids in the moving phase in dimensions $d > 2$, New J. Phys. **20**, 113035 (2018).

[21] A. Cavagna, L. Di Carlo, I. Giardina, T. S. Grigera, G. Pisegna, Equilibrium to off-equilibrium crossover in homogeneous active matter, Phys. Rev. Res. **3**, 013210 (2021).

[22] A. Cavagna, L. Di Carlo, I. Giardina, T. S. Grigera, S. Melillo, L. Parisi, G. Pisegna, M. Scandolo, Natural swarms in 3.99 dimensions, Nat. Phys. (2023), doi: 10.1038/s41567-023-02028-0.

[23] D. H. Kelley and N. T. Ouellette, Emergent dynamics of laboratory insect swarms, Sci. Rep. **3**, 1073 (2013).

[24] J. G. Puckett, R. Ni, and N. T. Ouellette, Time-Frequency Analysis Reveals Pairwise Interactions in Insect Swarms, Phys. Rev. Lett. **114**, 258103 (2015).

[25] R. Ni, J. G. Puckett, E. R. Dufresne, and N. T. Ouellette, Intrinsic Fluctuations and Driven Response of Insect Swarms, Phys. Rev. Lett. **115**, 118104 (2015).

[26] D. Gorbonos, R. Ianconescu, J. G. Puckett, R. Ni, N. T. Ouellette, and N. S. Gov, Long-range acoustic interactions in insect swarms: An adaptive gravity model, New J. Phys. **18**, 073042 (2016).

[27] M. Sinhuber and N. T. Ouellette, Phase Coexistence in Insect Swarms, Phys. Rev. Lett. **119**, 178003 (2017).

[28] Y. Feng and N. T. Ouellette, Non-uniform spatial sampling by individuals in midge swarms, J. R. Soc. Interface **20**, 20220521 (2023).

[29] A. M. Reynolds and N. T. Ouellette, Swarm dynamics may give rise to Lévy flights, Sci. Rep. **6**, 30515 (2016).

[30] A. M. Reynolds, F. Bartomeus, A. Kölzsch, and J. van de Koppel, Signatures of chaos in animal search patterns, Sci. Rep. **6**, 23492 (2016).

[31] R. Ni and N. T. Ouellette, Velocity correlations in laboratory insect swarms, Eur. Phys. J. Spec. Top. **224**, 3271 (2015).

[32] R. González-Albaladejo, A. Carpio, and L. L. Bonilla, Scale free chaos in the confined Vicsek flocking model, Phys. Rev. E **107**, 014209 (2023).

[33] T. Vicsek, A. Czirók, E. Ben-Jacob, I. Cohen, O. Shochet, Novel Type of Phase Transition in a System of Self-Driven Particles, Phys. Rev. Lett. **75**, 1226 (1995).

[34] H. Chaté, Dry aligning dilute active matter, Annu. Rev. Condens. Matter Phys. **11**, 189 (2020).

[35] D. J. Amit and V. Martin-Mayor, *Field Theory, The Renormalization Group and Critical Phenomena*, 3rd ed. (World Scientific, Singapore, 2005).

[36] J. B. Gao, J. Hu, W. W. Tung, Y. H. Cao, Distinguishing chaos from noise by scale-dependent Lyapunov exponent, Phys. Rev. E **74**, 066204 (2006).

[37] See Supplemental Material at http://link.aps.org/supplemental/10.1103/PhysRevE.107.L062601 for analytical and numerical calculations of the largest Lyapunov exponent, the order parameter, correlation length, susceptibility, and the critical exponents at $\eta = \beta = 0$, which includes three additional figures and Refs. [42–44].

[38] T. C. Halsey, M. H. Jensen, L. P. Kadanoff, I. Procaccia, and B. I. Shraiman, Fractal measures and their singularities: The characterization of strange sets, Phys. Rev. A **33**, 1141 (1986).

[39] E. Ott, *Chaos in Dynamical Systems* (Cambridge University Press, Cambridge UK, 1993).

[40] M. Cencini, F. Cecconi, and A. Vulpiani, *Chaos: From Simple Models to Complex Systems* (World Scientific, Singapore, 2010).

[41] K. Huang, *Statistical Mechanics*, 2nd ed. (Wiley, New York, 1987).

[42] G. Benettin, M. Casartelli, L. Galgani, A. Giorgilli, and J. M. Strelcyn, Lyapunov characteristic exponents for smooth dynamical systems and for hamiltonian systems: A method for computing all of them. Part 2: Numerical application, Meccanica **15**, 21 (1980).

[43] J. M. Greene and J.-S. Kim, The calculation of Lyapunov spectra, Physica D **24**, 213 (1987).

[44] S. N. Rasband, *Chaotic Dynamics of Nonlinear Systems* (Dover, New York, 1990).